Spatio-Temporal Entropy Analysis Of The Magnetic Field To Help Magnetic Cloud Characterization

Ojeda, G. A.,[1, 2] Mendes, O. ,[1] Calzadilla M. A,[2] and Domingues, M. O.[3]

Arian Ojeda González, Divisão de Geofísica Espacial-DGE, Coordenação Geral de Ciências Espaciais e Atmosféricas - CEA, Instituto Nacional de Pesquisas Espaciais - INPE, Av. dos Astronautas, 1.758 - Jd. Granja - São José dos Campos - SP - Brasil - CEP 12227-010. (arian@dge.inpe.br)

Odim Mendes Junior, Divisão de Geofísica Espacial-DGE, Coordenação Geral de Ciências Espaciais e Atmosféricas - CEA, Instituto Nacional de Pesquisas Espaciais - INPE, Av. dos Astronautas, 1.758 - Jd. Granja - São José dos Campos - SP - Brasil - CEP 12227-010.

Alexander Calzadilla Méndez, Departamento de Geofísica Espacial, Instituto de Geofísica y Astronomía - IGA, calle 212, 2906 e/ 29 y 31, La Coronela - La Lisa - Ciudad de la Habana - CUBA CP 11600.

Margarete Domingues Oliveira, Laboratório Associado de Computação e Matemática Aplicada, Coordenação de Laboratórios associados- CTE, Instituto Nacional de Pesquisas Espaciais - INPE, Av. dos Astronautas, 1.758 - Jd. Granja - São José dos Campos - SP - Brasil - CEP 12227-010.

[1]DGE/CEA/National Institute for Space

Abstract.

The aim of this work is to create a methodology to characterize the dynamics of magnetic clouds (MCs) from signals measured by satellites in the interplanetary medium. We have tested Spatio-Temporal Entropy (STE) technique to study 41 MCs identified by other authors, where the plasma sheath region has been identified. The STE was implemented in Visual Recurrence Analysis (VRA) software to quantify the order in the recurrence plot. Some tests using synthetic time series were performed to validate the method. In particular, we worked with IMF components B_x, B_y, B_z of 16 s. Time windows from March 1998 to December 2003 for some MCs were selected. We found higher STE values in the sheaths and zero STE values in some of the three components in most of the MCs (30 among 41 events). The trend is the principal cause of the lower STE values in the MCs. Also, MCs have mag-

Research - INPE 12227-010 São José dos Campos, SP, Brazil.

[2]Department of Space Geophysics, Institute of Geophysics and Astronomy - IGA Havana City, Cuba.

[3]LAC/CTE/National Institute for Space Research - INPE 12227-010 São José dos Campos, SP, Brazil.

netic field more structured than sheath and quiet solar wind. We have done a test considering the magnetic components of a cylindrically symmetric force-free constructed analytically, with the result of zero STE value. It agrees with the physical assumption of finding zero STE values when studying experimental data in MC periods. The new feature just examined here adds to the usual features, as described in Burlaga et al. [1981], for the characterization of MCs. The STE calculation can be an auxiliary objective tool to identify flux-ropes associated with MCs, mainly during events with no available plasma data but only with IMF.

1. Introduction

The term magnetic cloud (MC) has been used to characterize an Interplanetary Coronal Mass Ejection (ICME) that presents a specific configuration, in which the magnetic field strength is higher than average IMF, the magnetic field direction rotates smoothly through a large angle, and the proton temperature is low [Burlaga et al., 1981; Klein and Burlaga, 1982; Gosling, 1990]. Typically a flux-rope ejected from the Sun described the magnetic configuration of a MC. The MCs are observed in a clear way when the spacecraft crosses the magnetic field structure close by its center [Schwenn, 2006]. *In-situ* measurements are limited to the spacecraft trajectory crossing the incoming ICME. Therefore, one needs to rely on modeling evaluation in order to derive the global magnetic structure from available local measurements [Démoulin and Dasso, 2009]. Due to MCs moving faster than the surrounding solar wind (SW), plasmas and magnetic field typically accumulate in front of it, creating a preceding disturbed sheath.

In Ojeda et al. [2005], a study considering 20 MCs, 17 non-MC ICMEs, and 20 time series of equivalent time duration of quiet SW was done. The IMF B_z and solar wind V_x components in a time interval of 48 h before each MC were analyzed. Under MC conditions, a feature was identified that the component B_z of the IMF has the tendency to present lower spatio-temporal entropy (name given by Eugene Kononov's Visual Recurrence Analysis (VRA) software, not to be confused with spatio-temporal entropy image (STEI) [Ma and Zhang, 2001]) values than the B_z in other cases, such as in non-MC ICMEs and during quiet SW. This behavior seems to be very interesting under a physical point of view. Thus in this work a more detailed study of the spatio-temporal entropy

(STE) in MCs is carried out. The analyses are expanded to study the three magnetic components (B_x, B_y and B_z) using more complete dataset. The aim of this work is to validate the STE calculation technique as an useful tool to identify features of the MCs. A proposed approach to study the MCs by analyzing the time series of interplanetary magnetic field (IMF) is presented.

The content is organized as follows. In Section 2, a review on the theoretical and observational aspects of the interplanetary MCs is presented. In Section 3, the dataset used is described. In Section 4, a STE methodology for analyses is established. In Section 5, we compare STE values for time series corresponding to the MCs and the sheaths identified by Huttunen et al. [2005]. Finally, in Section 6 the conclusions are done. In Appendices, information on the tool is presented. Appendix A, shows a review on the tool in the VRA software. And Appendix B, the methods for calculating the entropy in the recurrence plot.

2. Magnetic Clouds

The pioneer studies on plasma clouds emitted by the Sun were developed about 1950s [Morrison, 1954; Cocconi et al., 1958; Piddington, 1958]. However the definition and the term of "magnetic cloud" were presented by the first time in the work of Burlaga et al. [1981]. Nowadays the specific signatures which have to be necessarily fulfilled are the following: (1) smooth rotation in $\vec{B}$ with low variance; (2) low proton temperature and (3) low plasma β, which is the ratio of the plasma pressure, $p = nk_BT$, to the magnetic pressure, $p_{mag} = B^2/2\mu_0$ where n is number density, K_B Boltzmann constant, T temperature, B magnetic field and μ_0 magnetic permeability of the free space.

Initial studies to analyze the three-dimensional configuration of the magnetic field of these phenomenon have been developed by Burlaga et al. [1981]. The minimum variance analysis (MVA) was used as a method to identify and describe planar magnetic field configuration associated with thin current sheets in the SW [Burlaga and Klein, 1980] and planetary magnetospheres [Lepping and Behannon, 1979]. Burlaga et al. [1981] used MVA to analyze the magnetic field configuration in a MC observed with 4 spacecraft: Voyager 1 and 2, IMP 8, and Helios 2. They concluded that MC could be represented as a magnetic cylinder whose axis lies close in the equatorial plane, marking an angle of nearly 90° with respect to the radial direction.

Considering a cylindrical geometry for MCs, the MVA [Sonnerup and Cahill, 1967] resulted an useful tool to calculate the direction of the cloud axis. Klein and Burlaga [1982] identified 45 events in the period between 1967 and 1978, where the latitude and longitude of the clouds axis were calculated. The results of Burlaga et al. [1981] also were consistent with other configurations. Ivanov and Harshiladze [1984] created a mathematical formulation using a cloud configuration as an oblate ellipsoidal. To understand how the magnetic field configuration evolves in the SW may be necessary for the correct interpretation of the field structure in MC [Burlaga and Behannon, 1982].

Goldstein [1983] considered a force-free configuration in the search for a stable topology of the MCs. Marubashi [1986] studied interplanetary magnetic field data from the Pioneer Venus orbiter (PVO) between December 1978 to May 1984 in search of interplanetary magnetic flux ropes near the Venus orbit. As a result, twenty-six well defined flux ropes were found which have characteristics similar to those of flux ropes observed near Earth. In one case, where the Sun, Venus and Earth were closely aligned, an almost identical structure was observed by the PVO and the Earth-orbiting spacecraft with a time delay of about 36 hours. This observation provides evidence that the structure of interplanetary magnetic flux ropes are maintained during propagation at least from 0.72 AU (Astronomical Unit (AU): The average distance from the Earth to the Sun. One AU = 93 million miles or 149.6 million km) to 1 *AU*. A simple solution for a cylindrically symmetric force-free field with constant alpha was studied by Lundquist [1950], and mentioned also in Lundquist [1951]. Burlaga [1988] studied the above solution with constant alpha to describe the types of signatures observed in the SW at 1 AU when MCs move past a spacecraft.

In order to find plasma beta values significantly lower than one to identify MCs, spacecraft measurements of magnetic field and plasma are required. Sometimes the temperature and density data on spacecraft have many gaps during periods in which the plasma instruments are saturated as a result of intense particle fluxes (for example, Bastille Day in the ACE spacecraft). If this condition occurs, it makes impossible to calculate the plasma beta, but it is still possible to detect the MC using magnetometers data [e.g., Huttunen et al., 2005; Nieves-Chinchilla et al., 2005]. Here is the contribution we intend to do with this work, showing an approach that could help to identify MCs, and it is proposed as basis for an auxiliary analysis tool.

The main contributions related to the identification of MCs are summarized in Table 1. It was adapted from Huttunen et al. [2005] and updated by us. We show in each column of this table, the paper, the period of the investigation, the examination period (T_t), the spacecraft used (Spacf), and the quantities number of MCs identified. Bothmer and Rust [1997]; Bothmer and Schwenn [1998]; Huttunen et al. [2005] identified MCs based on the MVA method; Mulligan et al. [1998] identified and classified MCs using the visual inspection of the data; Lynch et al. [2003] and Wu et al. [2003, /WIND list] used the least-square fitting routine by Lepping et al. [1990]; while Nieves-Chinchilla et al. [2005] studied all the MCs observed during the time interval $2000 - 2003$ using the elliptical cross-section model [Hidalgo, 2003, 2005], where a distortion and expansion of the cross-section of the cloud is included from first principles.

From 1997 – 2003 in solar cycle 23, SW data were investigated by Huttunen et al. [2005] using the MVA method [Sonnerup and Cahill, 1967; Bothmer and Schwenn, 1998] to determine if they have flux-rope structures. They identified 73 MCs observed by the ACE and WIND spacecraft. In principle the axis of a MC can have any orientation with respect to the ecliptic plane [Bothmer and Schwenn, 1994, 1998], identified by the azimuthal direction in the ecliptic, called ϕ_C, and the inclination relative to the ecliptic, called θ_C. With the MVA, the angles above can be calculated [Bothmer and Schwenn, 1998]. In order to classify MCs [Huttunen et al., 2005, and references therein], eight flux rope categories are often used , clustered as: Bipolar MCs (low inclination, and flux rope-type: SWN, SEN, NES, NWS), $\theta_C \leq 45\,^{\circ}$ and Unipolar MCs (high inclination, and flux rope-type: WNE, ESW, ENW, WSE), $\theta_C > 45\,^{\circ}$, where the meanings are S for south, N North, W west and E east.

Huttunen and collaborators have also included seven cloud candidate events for which either the fitting with MVA was not successful (e.g. the eigenvalue ratio < 2 or the directional change less than $30\,^{\circ}$) or there were large values of beta throughout the event. In their study, the criterion to identify a MC was based on the smoothness of the rotation in the magnetic field direction confined to one plane. Additionally they required that a

MC must have the average values of the plasma beta less than 0.5, the maximum value of the magnetic field at least 8 nT, and the duration at least 6 h. The last two criteria have been created with the objective of exclude "small and weak MCs". All selected events were investigated by analyzing 1 h magnetic field data with the minimum variance analysis (MVA), where MCs are identified from the smooth rotation of the magnetic field vector in the plane of the maximum variance [Klein and Burlaga, 1982]. For MCs with durations of 12 h or less Huttunen et al. [2005] performed MVA using 5-min (WIND) or 4-min (ACE) averaged data.

3. IMF Dataset

The IMF dataset used in this work are measurements obtained by the ACE satellite. The ACE spacecraft is in orbit around $L1$ from 1997 [Smith et al., 1998]. Where the Lagrangean point $L1$ is a gravitational equilibrium point between the Sun and Earth at about 1.5 million km from Earth and 148.5 million km from the Sun. On board of ACE a total of ten instruments, was launched toward L1 [McComas et al., 1998], but in this work only the Magnetic Field Experiment (MAG) is used. The MAG on board ACE consists of twin vector fluxgate magnetometers to measure the IMF [Smith et al., 1998]. The data ($http://www.srl.caltech.edu/ACE/ASC/level2/index.html$) contains time averages of the magnetic field over time periods 1 s, 16 s, 4 min, hourly, daily and 27 days (1 Bartels rotation). In this work, IMF components (B_x, B_y, B_z) with time resolution of 16 s in GSM coordinate systems are used.

We only work with 41 of 73 MCs identified by Huttunen et al. [2005] from March 1998 to December 2003: where the MCs were preceded by the plasma sheaths. We are interested in comparing these two regions when it have been well identified. The 41 events in chronological order are shown in Table 2 and 3. The columns from the left to the right give: a numeration of the events, year, shock time (UT), MC start time (UT) and MC end time (UT) respectively.

4. Methodology Using STE Analysis

Based on the description of MCs, a proper statistical tool can be used to identify their typical features. The STE analysis was chosen to establish a methodology. The STE analysis consists of a tool that compares the distribution of distances between all pairs of vectors in the reconstructed state space with that of distances between different orbits evolving in time. In this context, the terms “state space” and “orbits” are concepts of the theory of chaotic dynamical systems. State space reconstruction is the first step in non-linear time series analysis of data from chaotic systems including estimation of invariants and prediction. Dynamical regimes, such as a resting state or periodic oscillation, correspond to geometric objects, such as a point or a closed curve, in the phase space. Evolution of a dynamical system corresponds to a trajectory (or an orbit) in the phase space. Different initial states result in different trajectories. In the recurrence plot (RP) a one-dimensional time series from a data file is expanded into a higher-dimensional space, in which the dynamic of the underlying generator takes place. The concept of state space and orbit are also valid in the RP and in the subsequent calculation of the STE. The STE results identify in a certain objective way the characteristics of a physical process present in a time measurement dataset.

The VRA software provides resources to investigate this promising approach immediately. The recurrence plot has been used. For more details, the information on it is presented in Appendix A (recurrence plot) and Appendix B (entropy).

In this section, the purpose is to show the variation of STE values after processing carried out in some synthetic time series, file included in VRA software. The methodology to study synthetic time series will be implemented, with the purpose to be applied to analyse IMF dataset.

4.1. STE Variations Versus Trend Angle

From an intuitive point of view, a time series is said to be stationary if there has not trend and no systematic change in variance and if strictly periodic variations have been removed [Chartfield, 2003]. Trend estimation is a statistical technique that could be aid in the interpretation of data [Chartfield, 2003]. When a time series related to measurements of a process are treated, trend estimation can be used to make and justify statements about tendencies in the data. Given a set of data and the desire to produce some kind of function fitted through of those data the simplest function to fit is a straight line (using least-squares fit). If there is no global trend in time series the angle ("trend angle") between the straight line and the positive x axis must be zero.

We have calculated the STE value for each temporal series with embedding dimension and time delay equal to 1 respectively. It may be noticed that STE value changes for different embedding parameters. For example, for Lorenz attractor (Lorenz data file included in VRA), STE is near its minimum when the correct embedding is used (dimension $=3$, time delay $=16$ to this particular data file). This and other results suggest that STE can be used to determine the optimal embedding parameters, that is not the aim in this work. We selected the same embedding and time delay, equal to one, to maintain equivalence in the calculation of STE among all series in order to compare the results. Because our hypothesis is that this tool (STE) could be useful in a computational implementation to characterize MCs or used as a new property of them.

With the VRA software a group of synthetic time series were included. It were included a variety of time series with different properties, i.e. periodic, random, with noises and chaos respectively. A dataset of time series, Lorenz, Sine and White Noise, are used as test cases to validate the STE calculation.

Figure 1 shows a time series plot of Lorenz data file included in VRA software. We gave trends to the series through angular rotations about the origin. Time series have 3500 data records and it were rotated about the origin, angles of 0 rad, -0.01 rad, 0.01 rad and 0.0175 rad respectively. The STE values have been calculated for each time series and the results are shown in Table 4, row 2. In Table 4 in the five columns are shown: time series data file included in VRA version 4.7; these time series are rotated about the origin with the previous angles; and it is calculated the STE values of each time series.

We follow the same idea, to cause a trend in time series for another cases, Sine and White Noise data file also included in VRA software. The results have been included in rows 3 and 4 in Table 4. In periodic time series (sine data file) the STE value is always zero independently of increasing trend. In the other two cases, if time series trend increases then the STE values decreases (see row 2 and 4 in Table 4). We are doing those kinds of tests because we know that inside MCs the trend of IMF components increase; and we are interested in knowing how it could affect STE values.

To go on with the above idea is good to know that: the time series of the first difference is often enough to convert series with a trend into a stationary time series. The first-order differences of time series values $x_1,\ x_2,\ x_3, \cdots,\ x_N$ are given by a new series

$y_1,\ y_2,\ \cdots,\ y_{N-1}$, where $y_{N-1} = x_N - x_{N-1}$. The operation $y_t = x_t - x_{t-1} = \nabla x_t$ is called the first difference and ∇ is the difference operator [Chartfield, 2003].

Our interest is to study variations in the STE values when first-order differences are applied on stationary time series. In time series studied previously (Lorenz, Sine and White Noise), new time series from the first-order differences have been constructed. After that, we calculated STE values of each time series and the results were compared with the original series (non differentiated or untransformed) shown in Table 5. The STE values are similar in both of them, *i.e.*, for transformed (first-order differences) and untransformed time series. Thus, if the time series has non trend then the non-linear delicate structures are not destroyed.

The STE value is low and may tend to zero in any time series with trend. If there is a trend in the time series, it could be removed by differencing the original time series before calculating the STE. However, taking the first differences may interfere with the delicate nonlinear structure in the time series (if there is any). Thus STE values are calculated on the untransformed series and then in the transformed series, where the first-order differences is applied. This is done on a trial basis after calculating STE values of the original series.

4.2. Variations Of STE Values Given By Time Series Size

The calculation of the STE with the VRA software, version 4.7, can not be made in time series with size larger than $\sim$ 5000 points because the STE has a rapid decrease to zero. It seems to be a limitation of the software by some reason not explained in its tutorial. To exemplify the previous statement, synthetic series have been created using a pseudorandom number generator (PRNG) producing values in the range 0 to 1. In

Figure 2 (top panel), an example with 3000 points is shown. In this time series a STE value of 86% was calculated. The Figure 2 (bottom panel) shows the plot of STE values versus length(X(t)) of 18 time series constructed as shown in the top panel. The STE values decrease in time series with a length larger than $\sim$ 4000 points. When using the VRA software someone must take into account this identified limitation in the extension (length) of the data under analysis.

4.3. Scheme To Study STE Values In IMF Components

Figure 3 show the scheme that will be used to characterize MCs. From the 73 that have been identified by Huttunen et al. [2005] from March 1998 to December 2003 are selected 41 of them, the cases where the plasma sheath also is identified. For both regions, time series of IMF components with time resolution of 16 s, in GSM coordinates system, are selected. Using VRA software the data without transformations are processed. Also the same data before using the software are transformed. The aim of the transformations is to eliminate the trend and noises respectively. The trends are eliminated with two techniques, e.g. doing first order differences at time series and a rotation about the origin, in the beginning of this section both techniques were explained. To filter the white noise a Gaussian filter can be used, e.g. Mendes et al. [2006]. Inside the VRA software the RPs are generated and the STE values are calculated.

Using a simple solution for a cylindrically symmetric force-free field with constant alpha [Burlaga, 1988], time series were constructed. To a physical evaluation, the STE values are calculated. Finally, with the results, the MCs are characterized.

5. Results And Discussion

The STE values for the 41 MC events are shown in Figure 4. At the top, the STE values calculated from the three IMF components B_x, B_y and B_z, plotted respectively as " $\circ$ ", " $+$ " and " $\times$ ", corresponding to MCs. At the bottom, the same of above but for the sheath regions. The STE values of the 246 time series $(3*(41MCs+41Shts) = 246)$, were plotted in chronological order as appeared in Table 2 column 1. Some MCs do not have STE values close to zero in the three components simultaneously. Then, it is possible to find components with perfect structuredness (low STE) and absence of structure (high STE) in the same MC.

If STE values between the same components for the plasma sheath and the MC regions are compared (e.g. B_x-sheath ($STE = 56\%$) with B_x-cloud ($STE = 0\%$) in the event number 1), then in 5/41 (3/41) of the cases, in the B_x (B_y, B_z) component(s), the STE value in the MC is larger than at its plasma sheath region respectively. These are few cases, and show a clear tendency to decrease the STE value within the MC region in all IMF components. Someone can notice a clear tendency of the cloud events to present STE with lowest values, close to zero, as was noticed for B_z in Ojeda et al. [2005] and extended in this work, proposed as new feature adding to the usual features [Burlaga et al., 1981] established to the MCs.

Other interesting result is that STE values are zero in 20/41, 21/41, 26/41 MCs to B_x, B_y, B_z components respectively. The three components has zero entropy ($STE = 0\%$) at the same time in 17/41 MCs and 1/41 sheaths. The plasma sheath region with $STE = 0\%$ corresponds to event number 06 at Table 2.

Figure 5 shows a histogram of STE derived from Figure 4 for the B_z component corresponding to MCs (in black) and plasma sheaths (in grey) regions respectively. We have

37/41 or 90.2% of MCs with STE less than 40%. However, if we analyze the plasma sheath, then the result is exactly opposite, we found 37/41 or 90.2% of sheaths with STE larger than 40%. This shows the great difference between the two regions: the sheath is a turbulent region [Chian and Muñoz, 2011] where the plasma and magnetic field typically accumulate in ahead of the MC and cause fluctuations in the magnetic field. Thus, the time series could have more noise and therefore large STE values. In particular, the magnetic configuration of a MC could be described by a flux-rope with cylindrical geometry where the magnetic field has slow rotation along one day increasing the trend and decreasing the noise and therefore the STE values decrease. Low-entropy structures were found in the solar wind [e.g. Neugebauer et al., 2004], and physically we expected to find low entropy in the cloud. But the novel result shows that large amount of MCs with $STE = 0\%$ has been found.

We did some tests with time series to explain the above results. First, if the Gaussian noise is removed from the signal and the STE calculated, the STE value tend to decrease in less than 5% from its initial value. Second, when a trend is removed of the time series through a rotation (with the angle of slope line of best fit) the STE varies, but still the three components had $STE = 0\%$ at the same time in 17/41 MCs and 1/41 sheaths (see Figure 8, top panel). Third, by removing the trend through the first order difference in time series (see Figure 6). After that, there are still MCs with $STE = 0\%$.

In Figure 6 the study is the same as in Figure 4, but we have eliminated the trend through the first order difference in time series as mentioned in Section 4. In this case, most of calculating the STE values of all three components increased to $\sim 90\%$ in the plasma sheaths. Figure 7 shows a histogram of STE values in B_z component of MCs and sheaths derived from Figure 6. If we eliminate the trend in the time series, then the STE value increase. Leaving now 11 of a total of 27 MCs (see Figure 5) with STE values between 0% and 10%. Also the STE increases in the MC region, but there are still MCs with zero STE value.

Due to a software limitation, presented earlier (Figure 2), we investigated the effect of the length of the time series that have studied in Figure 4. Then, in Figure 8 (top panel), a plot of STE versus length of B_z time series for all MCs are shown. The " ◦ " and " + " symbols correspond to the original and transformed (removing the Gaussian noise and "trend" through a rotation about the origin) time series respectively. A vertical line was drawn in the point with $length(B_z) = 5500$ points. To the right of the vertical line, due to a software limitation (this was discussed in the end of section 4) the STE value is zero.

In Figure 8 (bottom panel) the histogram of the original or untransformed time series helps to identify overlapping points of MC that are shown in the top panel. Exist a total number of 17/41 MCs with zero STE values to the right of the vertical line. These are the events $1-4$, $6-10$, 13, 16, 27, 30, $33-35$, 40 shown in Table 2. This is a problem because the larger MCs are just the best structured. However, there still 9/41 MCs with zero STE values to the left of the vertical line, these are the events 5, 12, 21, $23-25$, 31, 32, 37 shown in Table 2. Event No. 38 has $STE = 6\%$ and complete the total of 27 events with STE between $0-10\%$ shown in the histogram at Figure 5.

In Figure 8 the STE values of the transformed time series (" + " symbol) increase and are different from zero in the MC with less than 5500 points. The smooth increase of trend occur in time series of IMF in a MC and is caused by the travel of an organized structure in form of flux-rope, crossing the spacecraft. The trend grows smoothly for the

IMF in a MC with length less than 5500 and are the main causes of lower STE values. Since the STE results of this tool can be affected by the trend, this tool could be useful in computational applications to identify MC regions, but failed to identify the boundaries of them.

In Figure 9 the study is the same as in Figure 8, but for the plasma sheaths regions. The length of the sheaths have less points than the MCs, only one sheath had more than 5500 points, the event number 6 shown in Table 2. Both histograms at the Figures 8 and 9 are constructed only to help in the visualization of the distribution of lengths at the top panels of it. The main result is that the STE values in the sheaths, of the transformed time series (“ + ” symbol), are approximately the same as the original (“ ◦ ” symbol) time series. We conclude that the trend in the plasma sheath is less important and STE have large values.

To study the true STE values of the MC with more than 5500 points and overcome the software limitation, we have two options: (1) select data with other temporal resolution (i.e., it to become poor the data information); or (2) select a MC sample with less than 5500 points. We performed option 2, taking the intervals from the positions 500 (to avoid effects caused by the identification of the boundaries) to 4500 in IMF B_z. Thus, the length of the time series reconstructed is 4001 data points. These 17/41 cases represented by “ × ” symbol are shown in Figure 10 (top panel); the “ ◦ ” symbol represent non-transform MCs similar to 8. In the right hand of the vertical line, the MCs sample (“ × ” symbol and 4001 data points) are plotted in the position with same length of non-transform MCs (“ ◦ ”). Only 1/17 case remains with zero STE and a total of 4/17 events remains with STE less than 11%. To make a better comparison, the histogram in the bottom panel at

Figure 10 was built. We have 33/41 or 80.5% of MCs with STE less than 40%. Still a good percentage (80.5%) that enables us to keep the findings of low STE in MCs.

A physical interpretation can be established as following. It was observed during the data processing that entropy values less than 40% could appear only in one or two of the three components of the MCs. This has a physical explanation: magnetic field axis of a magnetic flux-rope in a MC could have different inclinations. Then, the trend of IMF components is larger in a plane or one direction. It is advisable to work in a reference frame found by a MVA analysis. So far, we have been seeking the causes of the large amount of MCs with $STE = 0\%$. During a MC, the magnetic field strength is higher than the average, the magnetic field direction rotates smoothly through a large angle, then the periods with MCs present more trend in the magnetic behavior than the periods of sheaths or quiet SW. The trend is the principal cause of the lower STE values in MC.

To demonstrate quantitatively all results that have been shown up here, a simple solution for a cylindrically symmetric force-free field with constant alpha [Lundquist, 1950, 1951] was studied. Burlaga [1988] studied the above solution with constant alpha to describe the types of signatures observed in the SW at 1 AU when MCs travel through of a spacecraft. He concluded that the observed magnetic field profiles depend on the position and orientation of the axis of the MC. We written the force-free model solution as Burlaga [1988]:

$$\begin{aligned} \text{Axial component} : B_A &= B_0 J_0(\alpha R), \\ \text{Tangential component} : B_T &= B_0 H J_1(\alpha R), \\ \text{Radial component} : B_R &= 0, \\ \text{Total magnetic field} : B &= \sqrt{B_A^2 + B_T^2 + B_R^2}, \end{aligned} \tag{1}$$

where $H = \pm 1$, the sign providing the handedness of the field helicity, and where B_0 is an estimate of field at the axis of the cloud and R is the radial distance from the axis, J_0 and J_1 are the Bessel function of the first kind of order 0 and 1. The above equations were plotted in Figure 11. The magnitude of the magnetic field at any instant is B, which decreases from a maximum B_{max} on the axis of the MC to $\sim 0.5B_{max}$ at the outer boundary. Following Burlaga [1988], we show the boundaries with two vertical line in Figure 11 as the points where $B_A = 0$, i.e. where $\alpha \cdot R = 2.4$ and $B/B_0 = 0.5$.

Time series with 2001 points inside the boundaries of the cloud shown in Figure 11 are constructed. On other hand, we obtained the recurrence plots of B_A, B_T and B respectively. After that, the STE values are calculated; with the STE of $B_A = 27\%$; STE of $B_T = 0\%$; STE of $B = 25\%$.

Those low STE values are the physical justification of our results. If the spacecraft crosses near the cloud axis then zero entropy values of some IMF components of the structure are consequences of a nearly cylindrically symmetric force-free field. These results reinforce our initial hypothesis that STE could be established as a feature or tool to help in analysis of IMF data for the MC identification, mainly when the only measurements obtained by satellites are the IMF.

6. Conclusions

In this work, using the recurrence plot (RP) technique, a methodological approach is established in order to obtain the spatio-temporal entropy (STE) related to magnetic cloud (MC) periods. The method presented in Eugene Kononov's VRA software provides resource for this kind of analysis. For this investigation, the interplanetary magnetic fields from a complete solar wind data framework are investigated.

The analyses developed show that the STE values for MCs are lower than the ones for sheath region or the solar wind background.

The reason is that in MC the magnetic field strength is higher than the average, the magnetic field direction rotates smoothly through a large angle. Then periods of MCs have more trend than sheaths region and quiet SW periods. The trend is the principal cause of the lower values of STE. It can be noticed that inside MC the IMF have less fluctuations and less noise that outside its boundary. MCs have magnetic field more structured than sheath and quiet SW. This also collaborates for the decrease of STE within the MC region.

Also, the differences among the STE values for the three magnetic components in a MC give an idea about the anisotropy in the structure of MCs. Those features are related to the flux-rope structure orientation, based on concepts as presented by Bothmer and Schwenn [1994, 1998]. By using a force free model for IMF as presented by Burlaga [1988], a test considering the magnetic components, mainly the tangential component, of a cylindrically symmetric force-free field constructed analytically results zero STE value. It agrees with the physical assumption of finding zero STE values when studying experimental data in MC periods.

The new feature just examined here adds to the usual features, as described in Burlaga et al. [1981], for the characterization of MCs. Thus, the STE calculation can be an auxiliary objective tool to identify flux-ropes associated with MCs, mainly during events with no available plasma data but only with IMF.

Appendix A: The Recurrence Plots In Visual Recurrence Analysis Software

A summary of the ideas expressed in the Eugene Kononov's Visual Recurrence Analysis (VRA) software (VRA v4.7 http://nonlinear.110mb.com/vra/) about recurrence plots (RPs) is presented. In order to present the ideas, some figures are used to guide the description. Figure 12 (top panel) shows a recurrence plot (RP) for a simple sine wave, using the data file just included in VRA software. In it organized patterns of color characteristics are shown for the periodical signal. In order to allow a comparative view, a RP of white noise is shown in Figure 12 (bottom panel), with the data file also included. With a different result, an uniform distribution of color characteristics is noticed for the random signal.

The RP is a relatively recent technique for the qualitative assessment of time series [Eckmann et al., 1987]. This technique allows someone detects hidden patterns and structural changes in data or see similarities in patterns across the time series under analysis using graphical representation. The fundamental assumption underlying the idea is that an observable time series (a sequence of observations) is the manifestation of some dynamic process.

It has been proved mathematically that one can recreate a topologically equivalent picture of the original multidimensional system behavior by using the time series of a single observable variable [Takens, 1981]. The basic idea is that the effect of all the other (unobserved) variables is already reflected in the series of the observed output. Furthermore, the rules that govern the behavior of the original system can be recovered from its output.

In the RPs a one-dimensional time series from a data file is expanded into a higher-dimensional space, in which the dynamic of the underlying generator takes place. This is done by a technique called "delayed coordinate embedding", which recreates a phase space portrait of the dynamical system under study from a single (scalar) time series. To expand a one-dimensional signal into an M-dimensional phase space, one substitutes each observation in the original signal X(t) with vector $(y(i) = \{x(i), x(i-d), x(i-2d), \cdots, x(i-(m-1)d\})$, where i is the time index, m is the embedding dimension, d is the time delay. As a result, we have a series of vectors $Y = y(1), y(2), y(3), \cdots, y(N-(m-1)d)$, where N is the length of the original series.

With such reconstruction it is possible to reproduce the original system states at each time where we have an observation of that system output. Each unknown state $Z(t)$ at time t is approximated by a vector of delayed coordinates $Y(t) = x(t), x(t-d), x(t-2d), \cdots, x(t-(m-1)d$. After the Euclidean distances between all vectors are calculated, they are mapped to colors from the pre-defined color map and are displayed as colored pixels in their corresponding places (see Figure 12 (top panel), for example). The RP is a graphical representation of a correlation integral. The important distinction (and an advantage) is that the RP, unlike the correlation integrals, preserve the temporal dependence in the time series, in addition to the spatial dependence.

In RPs, if the underlying signal is truly random and has no structure, the distribution of colors is uniform and does not have any identifiable patterns (see Figure 12 (bottom panel), for example). There is some determinism in the signal generator, which can be detected by some distinctive color distribution. For example, hot colors (yellow, red, and orange) can be associated with small distances between the vectors, while others colors (blue, black) may be used to show large distances. In this printed work colors are noticed as a grey pattern (from white to black). Therefore one can visualize and study the motion of the system trajectories and infer some characteristics of the dynamical system that generated the time series. Also, the length of diagonal line segments of the same color on the RP brings an idea about the signal predictability. But, RP is mostly a qualitative tool.

For random signals, the uniform (even) distribution of colors over the entire RP is expected. The more deterministic the signal, the more structured the RP. So for the purpose of comparison in Figure 12 (top panel) the RP of a strictly periodic signal can see and in Figure 12 (bottom panel) the RP of the white noise time series.

For force-free model solution, the recurrence plots of B_A, B_T are shown at Figures 13, top and bottom panels respectively.

Appendix B: The Entropy Concepts In Recurrence Plot

The RP is a visual tool for the investigation of temporal recurrence in phase space [Takens, 1981]. With the purpose of reaching a quantitative tool in this work, a brief review about some methods to calculate the entropy in the RP and the phase space is presented here.

The calculation of the spatio-temporal entropy, called in short way as STE was used to measures the image "structuredness" in a bidimensional representation, *i.e.*, both in "space" and time domains. Its implementation in VRA software is to quantify the order found in RPs. The result is normalized and presented as a percentage of "maximum" entropy (randomness). When the entropy has a value of 100% it means the absence of any structure whatsoever (uniform distribution of colors, pure randomness, seen in Figure 12 (bottom panel)). In particular, 0% of entropy implies "perfect" structure (distinct color patterns, perfect "structuredness" and predictability, seen in Figure 12 (top panel)).

Recurrence is the most important feature of chaotic systems [Eckmann et al., 1987]. The popularity of RPs lies in the fact that their structures are visually appealing, and that they allow the investigation of high dimensional dynamics by means of a simple two-dimensional plot [Facchini et al., 2009]. For a better understanding and quantification of the recurrences, Webber and Zbilut [1994] have proposed a set of quantification measures, which are mainly based on the statistical distribution of the line structures in the RP. Recurrence quantification analysis (RQA) is a nonlinear technique used to quantify the information supplied by a RP [Zbilut and Webber, 1992; Webber and Zbilut, 1994]. Recurrence variables are calculated from the upper triangular area of the recurrence plot, excluding the central diagonal, because the plot is symmetrical about the main diagonal. The RQA can be used as a tool for the exploration of bifurcation phenomena and dynamics changes also in nonstationary and short time series. The entropy (ENT) is one of the recurrence variables of the RQA method. It is the Shannon information entropy for the distribution probability of the diagonal lines. That is:

$$ENT = - \sum_{k=L_{min}, p(k) \neq 0}^{L_{max}} p(k) log_2(p(k)), \tag{B1}$$

where L_{min} is the minimum length of diagonal lines in RP and

$$p(k) = \frac{\text{number of diagonal lines of length k in RP}}{\text{number of diagonal lines in RP}}. \tag{B2}$$

The ENT can be calculated using the VRA software; but it should not be confused with the STE.

Little et al. [2007] developed a Recurrence Period Density Entropy (RPDE) method, first it requires the embedding of a time series in phase space, which, according to Taken's embedding theorems, can be carried out by forming time-delayed vectors for each value x_n in the time series. Then, around each point in the embedded phase space, a recurrence neighbourhood of radius ϵ is created. All recurrences into this neighbourhood are tracked, and the time interval T between recurrences is recorded in a histogram. This histogram is normalized to create an estimate of the recurrence period density function p(T). The normalized entropy of this density is the RPDE value H_{norm} [Little et al., 2007].

$$H_{norm} = -(ln(T_{max}))^{-1} \sum_{t=1}^{T_{max}} p(t) ln(p(t)). \tag{B3}$$

The RPDE value is a scalar in the range zero to one. For purely periodic signals, $H_{norm} = 0$ (STE=0%) whereas for purely uniform white noise, $H_{norm} = 1$ (STE=100%). However, estimates obtained with this technique (RPDE) are different from those obtained with the STE.

Dasan et al. [2002] report an analysis, using the tools of nonlinear dynamics and chaos theory, of the fluctuations in the stress determined from simulations of shear flow of Stokesian suspensions. They also computed the STE using VRA for the stress. The calculated values of the STE for the shear and normal stresses were nearly zero, showing perfect structure in the data. They observed definite structure in the phase-space plot of the stress components [Dasan et al., 2002]. They cited the works of Peacock [1983]; Carr and Schwartz [1998]. Peacock [1983] presented a two-dimensional analogue of Kolmogorov-

Smirnov test, useful for analysing the distribution of data in two dimensions, as is the RP. Carr and Schwartz [1998] investigated the fluctuation phenomena in plasmas that often needs the analysis of spatio-temporal signals. It was shown how such signals can be analyzed using the biorthogonal decomposition, which splits them into orthogonal spatial and temporal modes. Several parameters allow one to quantify the weight distribution in the biorthogonal decomposition. The total energy of spatio-temporal signal is found to be equal to the sum of the eigenvalues, α_m:

$$E(u) = \sum_{m=1}^{N} \alpha_m^2. \tag{B4}$$

They can define the relative energy of the m^{th} structure as

$$E_m(u) = \frac{\alpha_m^2}{E(u)}, \tag{B5}$$

and the entropy of the spatio-temporal signal $u(t, j)$ is defined as

$$H(u) = -\frac{1}{logN} \sum_{m=1}^{N} E_m(u) log E_m(u). \tag{B6}$$

It describes how the energy is distributed across the N_s significant structures. Signal whose energy is concentrated in a single structure such that $N_s = 1$ will have very low entropy $H(u) = 0$, or $H(u) = 1$ if the energy is distributed equally among the N_s significant structures. Further, the results presented in this paper shows the usefulness of STE implemented by Eugene Kononov's software to study MCs.

Acknowledgments. This work was supported by grants from CNPq (grants 483226/2011-4, 307511/2010-3, 306828/2010-3 and 486165/2006-0), FAPESP (grants 2012/072812-2 and 2007/07723-7) and CAPES (grants 1236-83/2012 and 86/2010-29). Arian Ojeda González thanks the CAPES and CNPq (grant 141549/2010-6) for his PhD scholarship and CNPq (grant 150595/2013-1) for his postdoctoral research support. We are grateful to V. E. Menconni (FAPESP grant 2008/09736-1) for their helpful computational assistance. We also wish to thank the anonymous referees for improvement of this paper. Acknowledgments to Eugene Kononov, author of the Visual Recurrence Analysis software. Also, the authors would like to thank ACE science team members for the datasets used in this work.

References

Bothmer, V., Rust, D. M., 1997. The field configuration of magnetic clouds and the solar cycle. Geophysical Monograph99, 139–146, AGU.

Bothmer, V., Schwenn, R., 1994. Eruptive prominences as sources of magnetic clouds in the solar wind. Space Science Reviews 70, 215.

Bothmer, V., Schwenn, R., 1998. The structure and origin of magnetic clouds in the solar wind. Annales Geophysicae 16, 1–24, 10.1007/s00585-997-0001-x.

Burlaga, L., Behannon, K., 1982. Magnetic clouds: Voyager observations between 2 and 4 AU. Solar Physics 81, 181.

Burlaga, L. F., 1988. Magnetic clouds and force-free fields with constant alpha. Journal of Geophysical Research 93 (7), 7217–7224.

Burlaga, L. F., Klein, L. W., Mar. 1980. Magnetic clouds in the solar wind. NASA Tech. Memo (80668), 1–15.

Burlaga, L. F., Sittler, E., Mariani, F., Schwenn, R., 1981. Magnetic loop behind an interplanetary shock: Voyager, Helios and IMP 8 observations. Journal of Geophysical Research 86, 6673–6684.

Carr, T. W., Schwartz, I. B., 1998. On measures of disorder in globally coupled oscillators. Physica D 115, 321–340.

Chartfield, C., Jul. 2003. The analysis of time series an introduction, sixth Edition. Chapman & Hall/CRC Texts in Statistical Science). Taylor & Francis e-Library, 2009.

Chian, A. C.-L., Muñoz, P. R., 2011. Detection of Current Sheets and Magnetic Reconnections at the Turbulent Leading Edge of an Interplanetary Coronal Mass Ejection. The Astrophysical Journal Letters 733 (2), L34.

Cocconi, G., Greisen, K., Morrison, P., Gold, T., Hayakawa, S., 1958. The cosmic ray flare effect. Il Nuovo Cimento(1955-1965) 8, 161–168.

Dasan, J., Ramamohan, T. R., Singh, A., Nott, P. R., 2002. Stress fluctuations in sheared Stokesian suspensions. Physical Review E 66 (2), 021409.

Démoulin, P., Dasso, S., May 2009. Causes and consequences of magnetic cloud expansion. Astronomy and Astrophysics 498 (2), 551–566.

Eckmann, J., Kamphorst, S., Ruelle, D., 1987. Recurrence plots of dynamical systems. Europhysics Letters 4 (9), 973–977.

Facchini, A., Mocenni, C., Vinicio, A., 2009. Generalized recurrence plots for the analysis of images from spatially distributed systems. Physica D 238, 162–169.

Goldstein, H., 1983. On the field configuration in magnetic clouds. Solar Wind Five, 731.

Gosling, J., 1990. Coronal mass ejections and magnetic flux ropes in interplanetary space. In: Russel, C. T., Priest, E. R., Lee, L. C. (Eds.), Physics of Magnetic Flux Ropes. AGU Geophys. Monogr., p. 343.

Hidalgo, M. A., 2003. A study of the expansion and distortion of the cross section of magnetic clouds in the interplanetary medium. Journal of Geophysical Research 108 (A8).

Hidalgo, M. A., Mar. 2005. Correction to “A study of the expansion and distortion of the cross section of magnetic clouds in the interplanetary medium”. Journal of Geophysical Research (Space Physics) 110, 3207.

Huttunen, K. E. J., Bothmer, V., Koskinen, H. E. J., 2005. Properties and geoeffectiveness of magnetic clouds in the rising, maximum and early declining phases of solar cycle 23. Annales Geophysicae 23, 1–17.

Ivanov, K., Harshiladze, A., 1984. Dynamics of hydromagnetic clouds from powerful solar flares. Solar Physics 92, 351.

Klein, L. W., Burlaga, L. F., 1982. Interplanetary magnetic clouds at 1 AU. Journal of Geophysical Research 87, 613–624.

Lepping, R. P., Behannon, K. W., Jun. 1979. Magnetic field directional discontinuities. 1: Minimum variance errors. NASA STI/Recon Technical Report N 79, 31116.

Lepping, R. P., Burlaga, L. F., Jones, J. A., Aug. 1990. Magnetic field structure of interplanetary magnetic clouds at 1 AU. Journal of Geophysical Research 951, 11957–11965.

Little, M. A., McSharry, P. E., J., R. S., Costello, D. A., Moroz, I. M., 2007. Exploiting Nonlinear Recurrence and Fractal Scaling Properties for Voice Disorder Detection. BioMedical Engineering OnLine.

Lundquist, S., 1950. Magnetohydrostatic fields. Ark Fys 2, 361–365.

Lundquist, S., Jul. 1951. On the Stability of Magneto-Hydrostatic Fields. Physical Review 83, 307–311.

Lynch, B., Zurbuchen, T., Fisk, L., Antiochos, S., 2003. Internal structure of magnetic clouds: Plasma and composition. Journal of Geophysical Research 108 (A6), 1239–1253.

Ma, Y., Zhang, H., 2001. Detecting motion object by Spatial-Temporal Entropy. In: IEEE International Conference on Multimedia and Expo, 2001. pp. 265–268.

Marubashi, K., 1986. Structure of the interplanetary magnetic clouds and their solar origins. Advances in Space Research 6 (6), 335–338.

McComas, D. J., Bame, S. J., Barker, P., Feldman, W. C., Phillips, J. L., Riley, P., Griffee, J. W., Jul. 1998. Solar Wind Electron Proton Alpha Monitor (SWEPAM) for the Advanced Composition Explorer. Space Science Reviews 86, 563–612.

Mendes, O., Mendes da Costa, A., Bertoni F., 2006. Effects of the number of stations and time resolution on Dst derivation. Journal of Atmospheric and Solar-Terrestrial Physics 68(18):2127-2137, doi: 10.1016/j.jastp.2006.01.015.

Morrison, P., 1954. Solar-connected variations of the cosmic rays. Physical Reviews 95, 646.

Mulligan, T., Russel, C. T., Luhmann, J., 1998. Solar cycle evolution of the structure of magnetic clouds in the inner Heliosphere. Geophysical Research Letters 25 (15), 2959–2962.

Neugebauer, M., Liewer, P. C., Goldstein, B., Zhou, X., Steinberg, J. T., Oct. 2004. Solar wind stream interaction regions without sector boundaries. Journal of Geophysical Research 109 (A10102), 102.

Nieves-Chinchilla, T., Hidalgo, M., Sequeiros, J., 2005. Magnetic Clouds Observed at 1 Au During the Period 2000–2003. Solar Physics 232, 105–126.

Ojeda, G. A., Calzadilla, A., Lazo, B., Alazo, K., Savio, S., 2005. Analysis of Behavior of Solar Wind Parameters Under Different IMF Conditions Using Two Nonlinear Dynamics Techniques. Journal of Atmospheric and Solar-Terrestrial Physics 67, 1859–1864.

Peacock, J. A., Feb. 1983. Two-dimensional goodness-of-fit testing in astronomy. Royal Astronomical Society 202 (1983), 615–627.

Piddington, J. H., 1958. Interplanetary Magnetic Field and Its Control of Cosmic-Ray Variations. Physical Reviews 112, 589.

Sonnerup, B., Cahill, L., 1967. Magnetopause structure and attitude from Explorer 12 observations. Journal of Geophysical Research 72, 171.

Schwenn, R., 2006. Space weather: The Solar Perspective. Living reviews in solar physics 3 (2), 1–72.

Smith, C. W., L'Heureux, J., Ness, N. F., Acuña, M. H., Burlaga, L. F., Scheifele, J., 1998. The ACE Magnetic Fields Experiment. Space Science Reviews, v. 86, p. 613–632.

Takens, F., 1981. Detecting strange attractors in turbulence. Lecture Notes in Mathematics, 366–381.

Webber, C. L., Zbilut, L. P., 1994. Dynamical assessment of physiological systems and state using recurrence plot strategies. Journal of Applied Physiology 76, 965–973.

Wu, C.-C., Lepping, R. P., Gopalswamy, N., Sep. 2003. Variations of magnetic clouds and CMEs with solar activity cycle. In: Wilson, A. (Ed.), Solar Variability as an Input to the Earth's Environment. Vol. 535 of ESA Special Publication. pp. 429–432.

Zbilut, L. P., Webber, C. L., 1992. Embeddings and delays as derived from quantification of recurrence plots. Physics Letters A 171, 199–203. 2101

Table 1. Summary of seven previous studies that identified MCs before 2003. In column one: 1- Bothmer and Rust [1997], 2- Bothmer and Schwenn [1998], 3- Mulligan et al. [1998], 4- Lynch et al. [2003], 5- Wu et al. [2003],6- Huttunen et al. [2005], 7- Nieves-Chinchilla et al. [2005].

Paper	Period	T_t(years)	Spacf	MC
1	1965-1993	28	OMNI	67
2	12/1974-07/1981	6.7	Helios 1/2	45
3	1979-1988	10	Pioneer	61
4	02/1998-07/2001	3.5	ACE	56
5	1995-2002	8	WIND	71
6	1997-2003	7	WIND/ACE	73
7	2000-2003	4	WIND/ACE	35

[a] SOURCE: Adapted from Huttunen et al. [2005].

Table 2. Solar Wind data studied (from Huttunen et al. [2005]).

No.	Year	Shock	UT	Start	UT	Stop	UT
01	1998	06 Jan	13:19	07 Jan	03:00	08 Jan	09:00
02		03 Feb	13:09	04 Feb	05:00	05 Feb	14:00
03		04 Mar	11:03	04 Mar	15:00	05 Mar	21:00
04		01 May	21:11	02 May	12:00	03 May	17:00
05		13 Jun	18:25	14 Jun	02:00	14 Jun	24:00
06		19 Aug	05:30	20 Aug	08:00	21 Aug	18:00
07		24 Sep	23:15	25 Sep	08:00	26 Sep	12:00
08		18 Oct	19:00	19 Oct	04:00	20 Oct	06:00
09		08 Nov	04:20	08 Nov	23:00	10 Nov	01:00
10		13 Nov	00:53	13 Nov	04:00	14 Nov	06:00
11	1999	18 Feb	02:08	18 Feb	14:00	19 Feb	11:00
12		16 Apr	10:47	16 Apr	20:00	17 Apr	18:00
13		08 Aug	17:45	09 Aug	10:00	10 Aug	14:00
14	2000	11 Feb	23:23	12 Feb	12:00	12 Feb	24:00
15		20 Feb	20:57	21 Feb	14:00	22 Feb	12:00
16		11 Jul	11:22	11 Jul	23:00	13 Jul	02:00
17		13 Jul	09:11	13 Jul	15:00	13 Jul	24:00
18		15 Jul	14:18	15 Jul	19:00	16 Jul	12:00
19		28 Jul	05:53	28 Jul	18:00	29 Jul	10:00
20		10 Aug	04:07	10 Aug	20:00	11 Aug	08:00
21		11 Aug	18:19	12 Aug	05:00	13 Aug	02:00
							Continue

Table 3. Continuation of Table 2.

No.	Year	Shock	UT	Start	UT	Stop	UT
22		17 Sep	17:00	17 Sep	23:00	18 Sep	14:00
23		02 Oct	23:58	03 Oct	15:00	04 Oct	14:00
24		12 Oct	21:36	13 Oct	17:00	14 Oct	13:00
25		28 Oct	09:01	28 Oct	24:00	29 Oct	23:00
26		06 Nov	09:08	06 Nov	22:00	07 Nov	15:00
27	2001	19 Mar	10:12	19 Mar	22:00	21 Mar	23:00
28		27 Mar	17:02	27 Mar	22:00	28 Mar	05:00
29		11 Apr	15:18	12 Apr	10:00	13 Apr	06:00
30		21 Apr	15:06	21 Apr	23:00	22 Apr	24:00
31		28 Apr	04:31	28 Apr	24:00	29 Apr	13:00
32		27 May	14:17	28 May	11:00	29 May	06:00
33		31 Oct	12:53	31 Oct	22:00	02 Nov	04:00
34	2002	23 Mar	10:53	24 Mar	10:00	25 Mar	12:00
35		17 Apr	10:20	17 Apr	24:00	19 Apr	01:00
36		18 May	19:44	19 May	04:00	19 May	22:00
37		01 Aug	23:10	02 Aug	06:00	02 Aug	22:00
38		30 Sep	07:55	30 Sep	23:00	01 Oct	15:00
39	2003	20 Mar	04:20	20 Mar	13:00	20 Mar	22:00
40		17 Aug	13:41	18 Aug	06:00	19 Aug	11:00
41		20 Nov	07:27	20 Nov	11:00	21 Nov	01:00

END

Table 4. STE values related to trends for three time series with data file included in VRA 4.7.

Series/angle (rad)	0	-0.01	0.01	0.0175
STE(Lorenz):	73%	30%	29%	0%
STE(Sine):	0%	0%	0%	0%
STE(White Noise):	80%	34%	34%	3%

Table 5. STE values related to the first-order differences in time series.

Series	Untransformed	first-order differences
STE(Lorenz)	73%	75%
STE(Sine)	0%	0%
STE(White Noise)	80%	82%

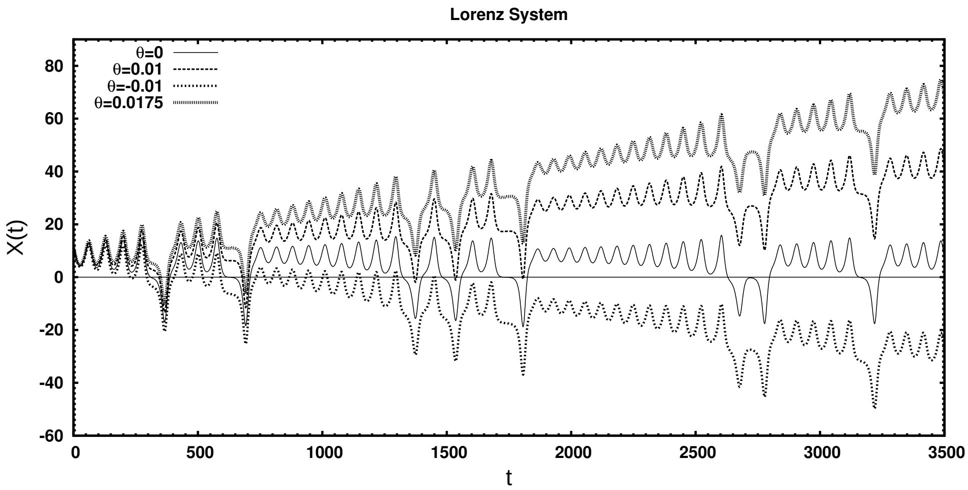

Figure 1. Time series plot of Lorenz data file included in VRA (case with $\theta = 0$). Series rotated about origin ($\theta = -0.01$ rad , $\theta = 0.01$ rad , $\theta = 0.0175$ rad) and the three resulting series also plotted. After that, we calculate the STE of each time series.

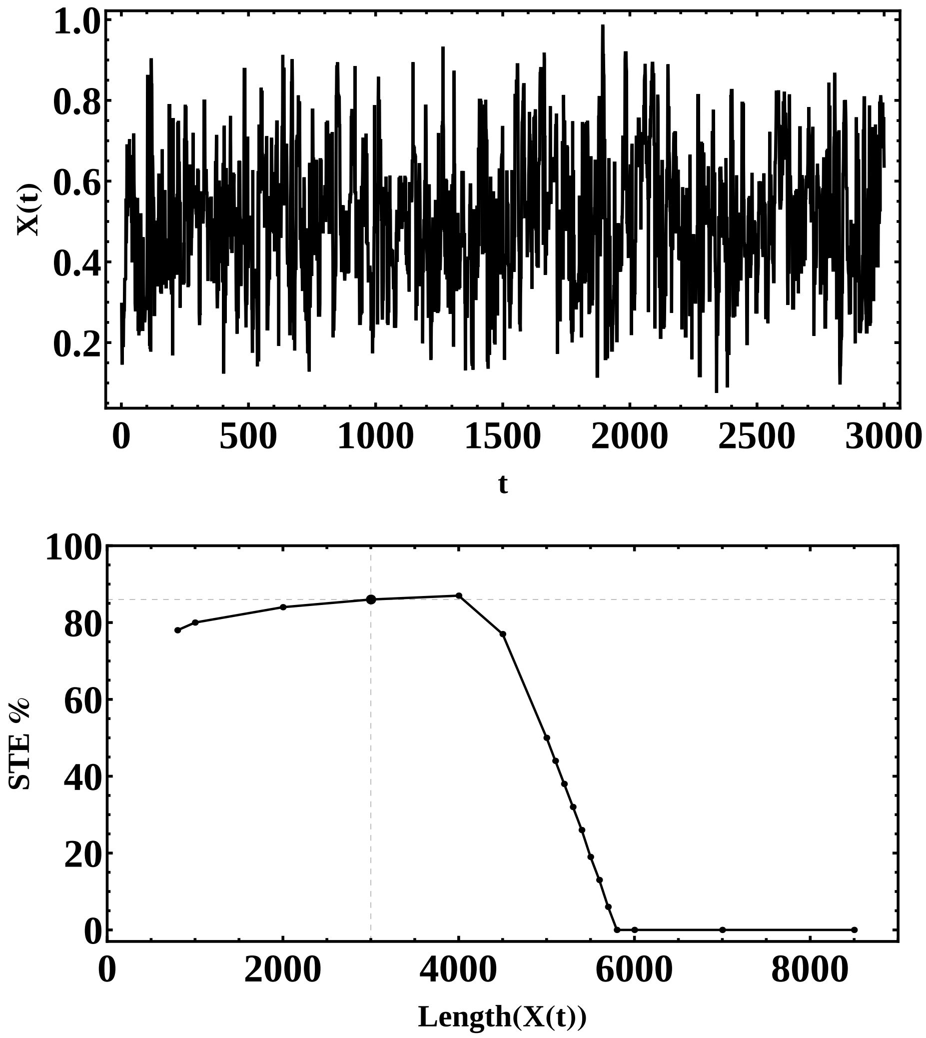

Figure 2. (top panel) X(t) vs t is plotted, where X(t) is a synthetic series created using a pseudorandom number generator producing values in the range 0 to 1. A simple moving average is applied to show the graph. The time series of pseudorandom number has a recurrence plot similar to shown at Figure 12 (bottom panel) and STE value of this time series is 86%. (bottom panel) The STE values versus length(X(t)) of time series constructed. These values decrease in time series with a length larger than $\sim$ 4000 points.

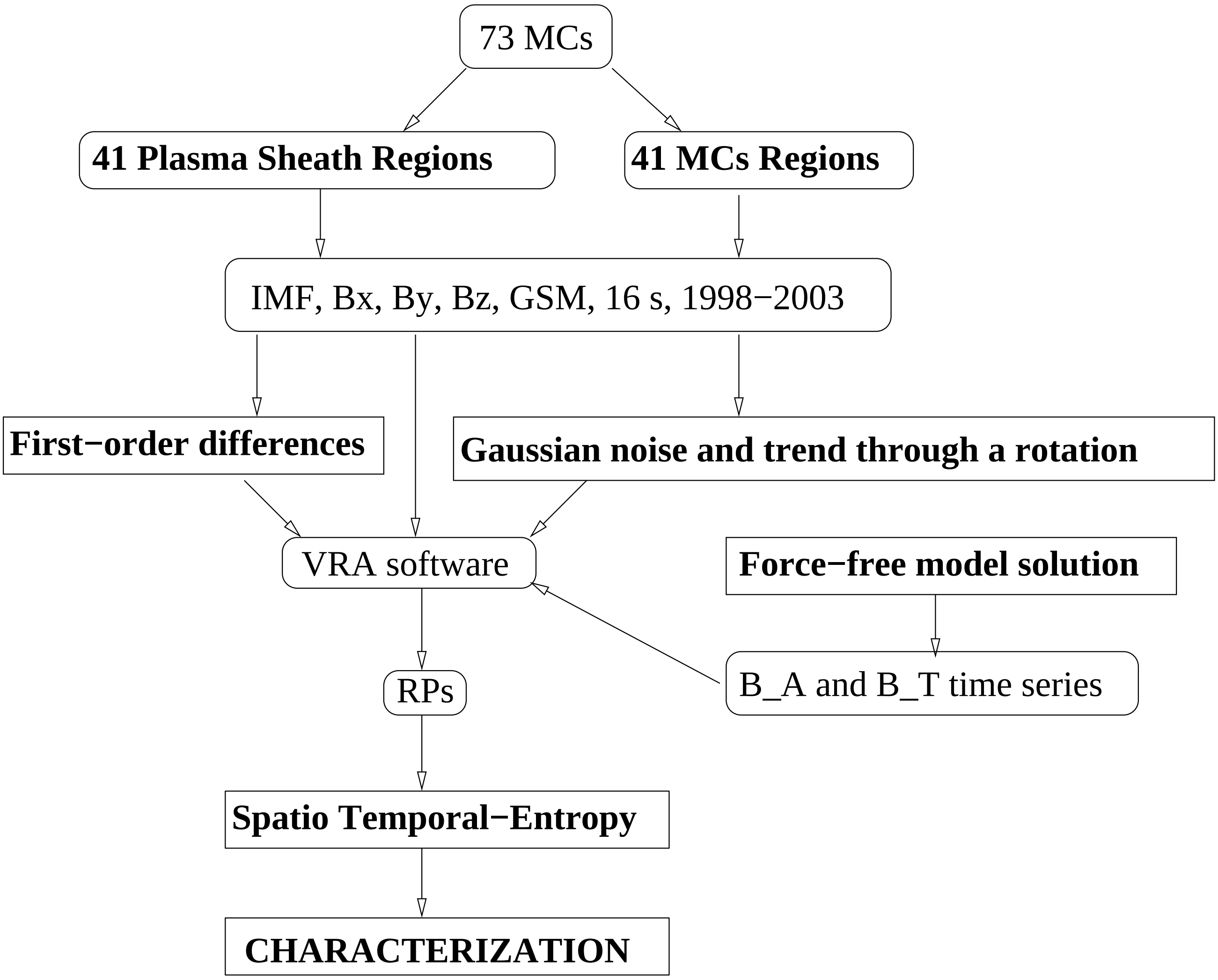

Figure 3. Scheme used to study 41 MCs in Section 5.

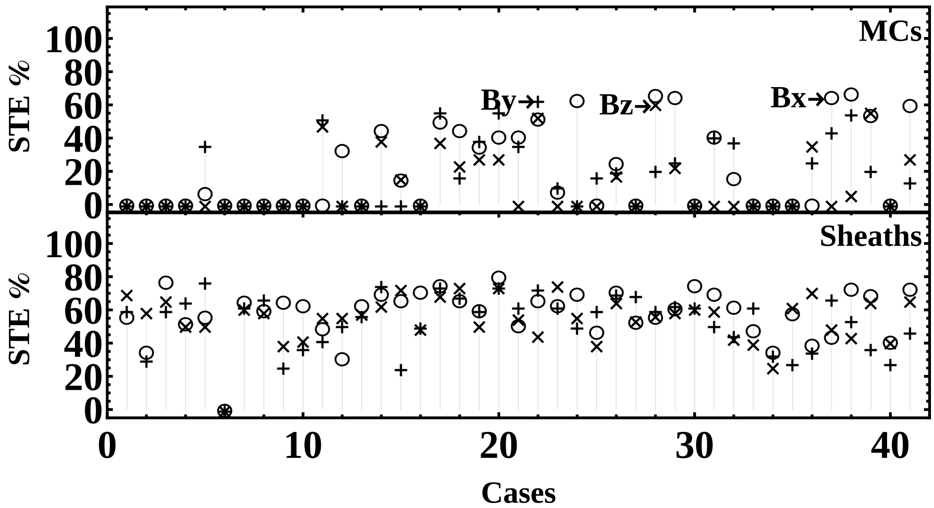

Figure 4. The STE values for 41 MCs from 1998 to 2003 that were presented in Table 2. At the top, the STE values for the three IMF components ("$\circ$" $\equiv B_x$, "$+$" $\equiv B_y$, "$\times$" $\equiv B_z$) versus cases as shown in Table 2. At bottom, the same as to above but for the sheath regions. In the two panels without previous transformation in the time series.

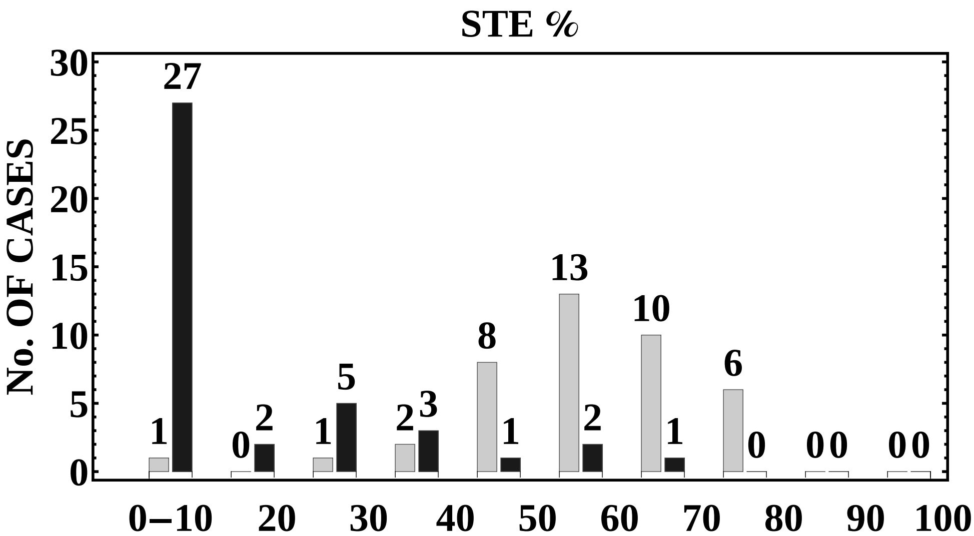

Figure 5. A histogram of STE derived from Figure 4 for B_z corresponding to MCs regions (in black) and plasma sheaths regions (in grey) respectively.

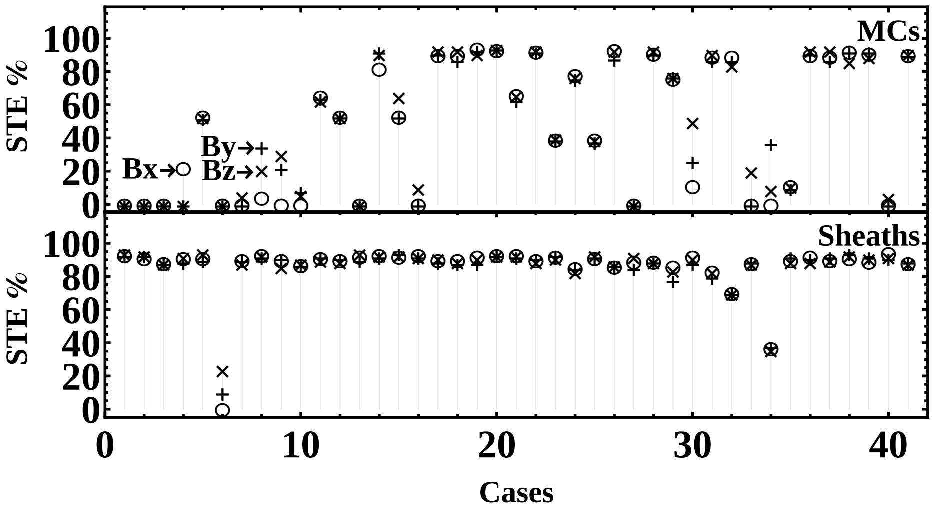

Figure 6. Format is the same as in Figure 4, but the trend was removed through the first-order differences at the time series.

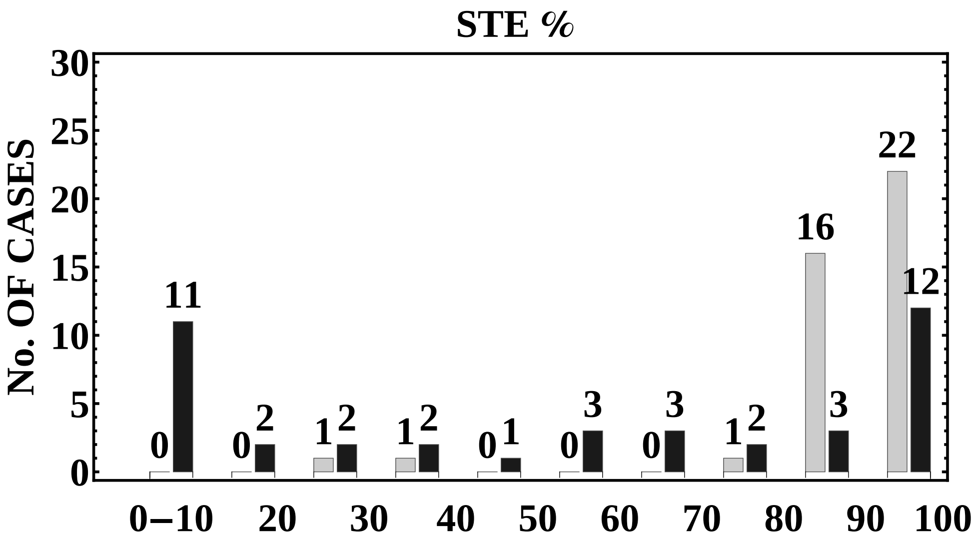

Figure 7. A histogram of STE derived from Figure 6 for B_z corresponding to MCs regions (in black) and plasma sheaths regions (in grey) respectively.

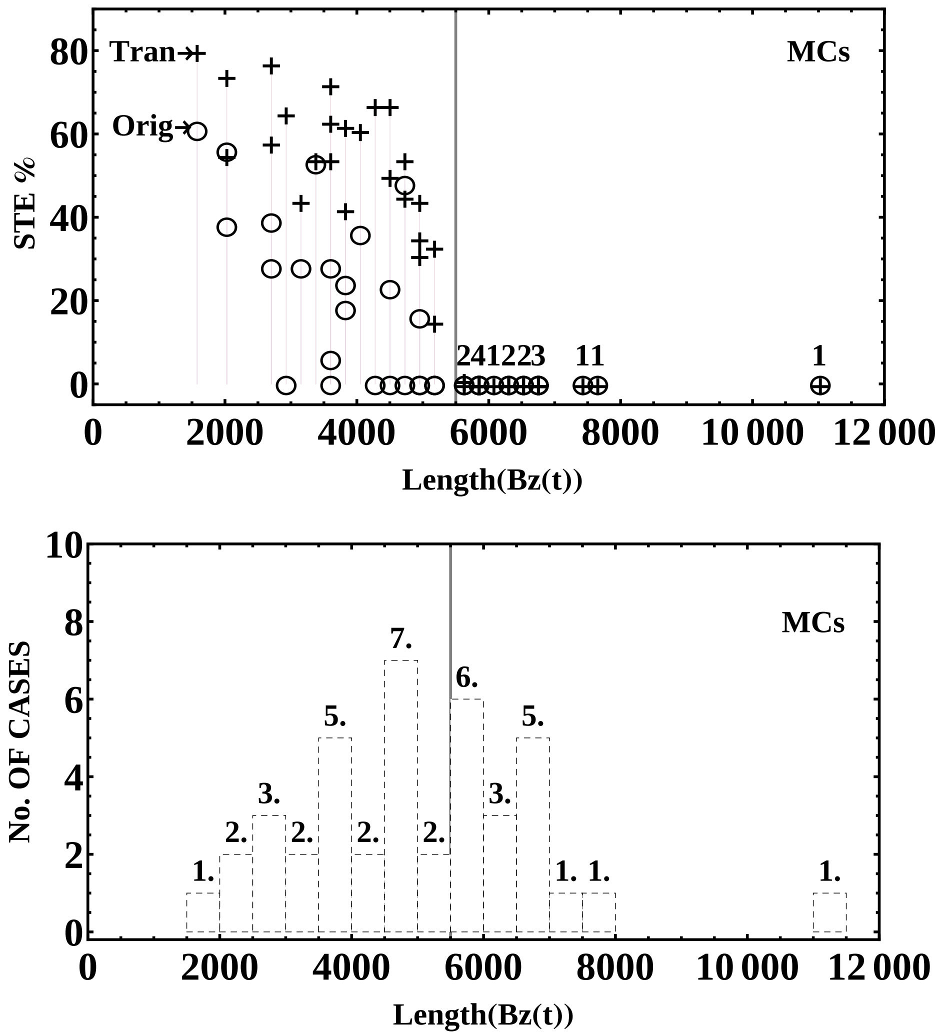

Figure 8. (top panel) STE values versus length of B_z time series using 41 MCs, where the "$\circ$" and "$+$" symbols corresponds to original and transformed (remove the Gaussian noise and trend through a rotation) time series respectively. To the right of the vertical line, larger clouds are shown, and by the software limitation the STE values are zero. (bottom panel) The histogram helps to identify overlapping points of MCs in the top panel.

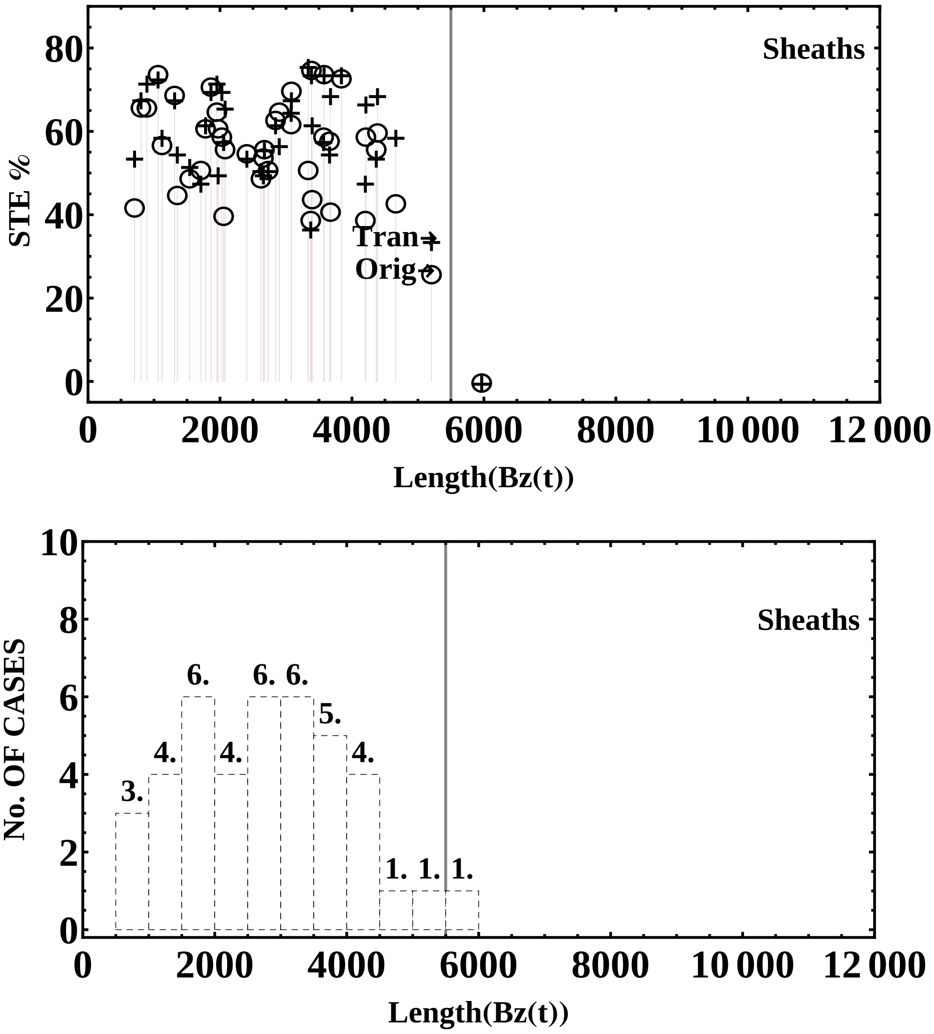

Figure 9. In both panels, the format is the same as in Figure 8, but STE values 41 plasma sheaths are plotted. (bottom panel) The histogram helps to identify overlapping points of sheaths in the top panel.

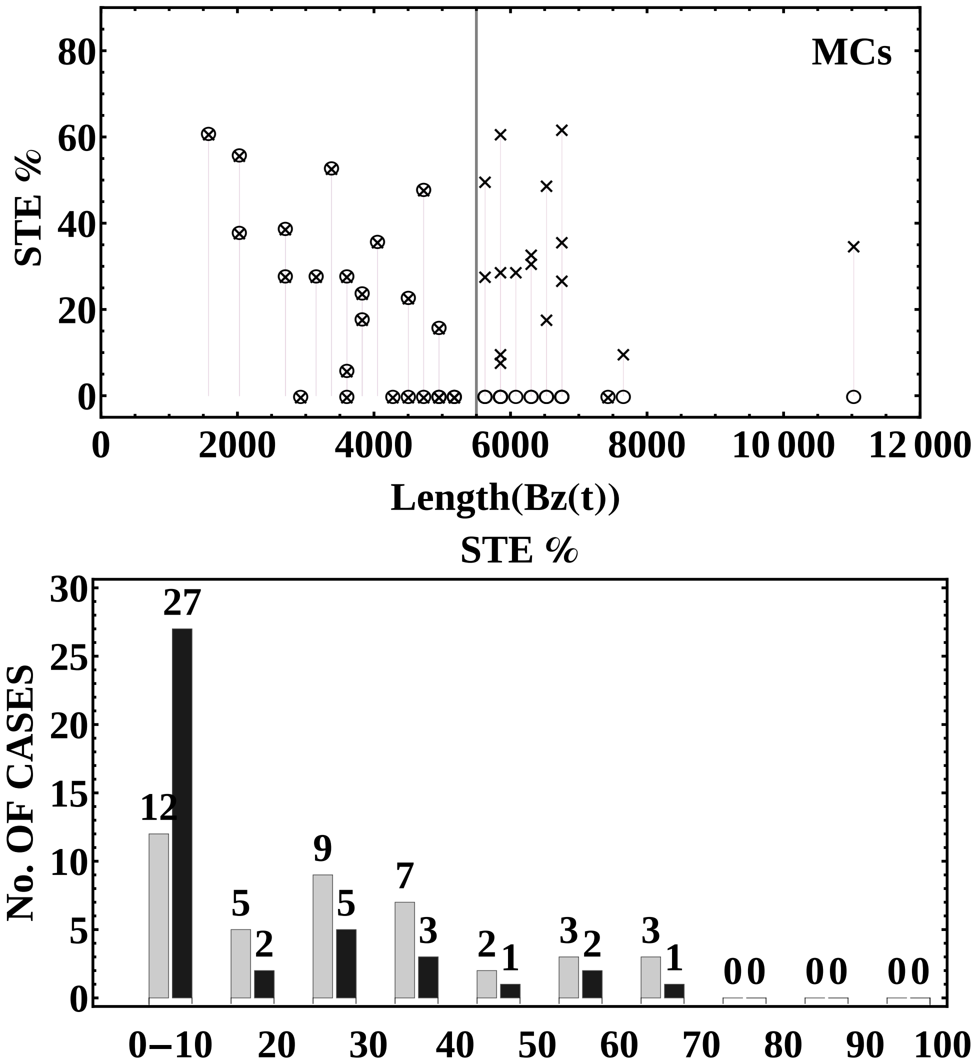

Figure 10. We selected MCs sample with less of 5500 points, taking the intervals between the positions 500 until 4500 in IMF B_z. (top panel) The " $\circ$ " and " $\times$ " symbols correspond to non-transform and transformed (reduced to 4001 points) time series respectively. (bottom panel) A histogram of STE derived from top panel corresponding to transformed (in grey) and non-transform (in black) of B_z time series.

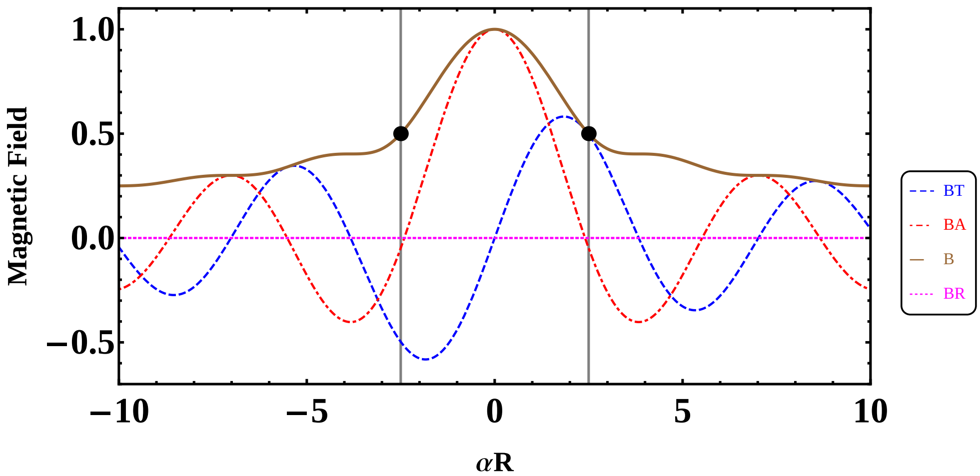

Figure 11. The force-free model solution (axial, tangential and radial components and total magnetic field) as solved in Burlaga [1988] were plotted. Following Burlaga [1988], we show the boundaries with two vertical lines at the points where $B_A = 0$, i.e. where $\alpha \cdot R = 2.4$ and $B/B_0 = 0.5$, also $\alpha = 1$.

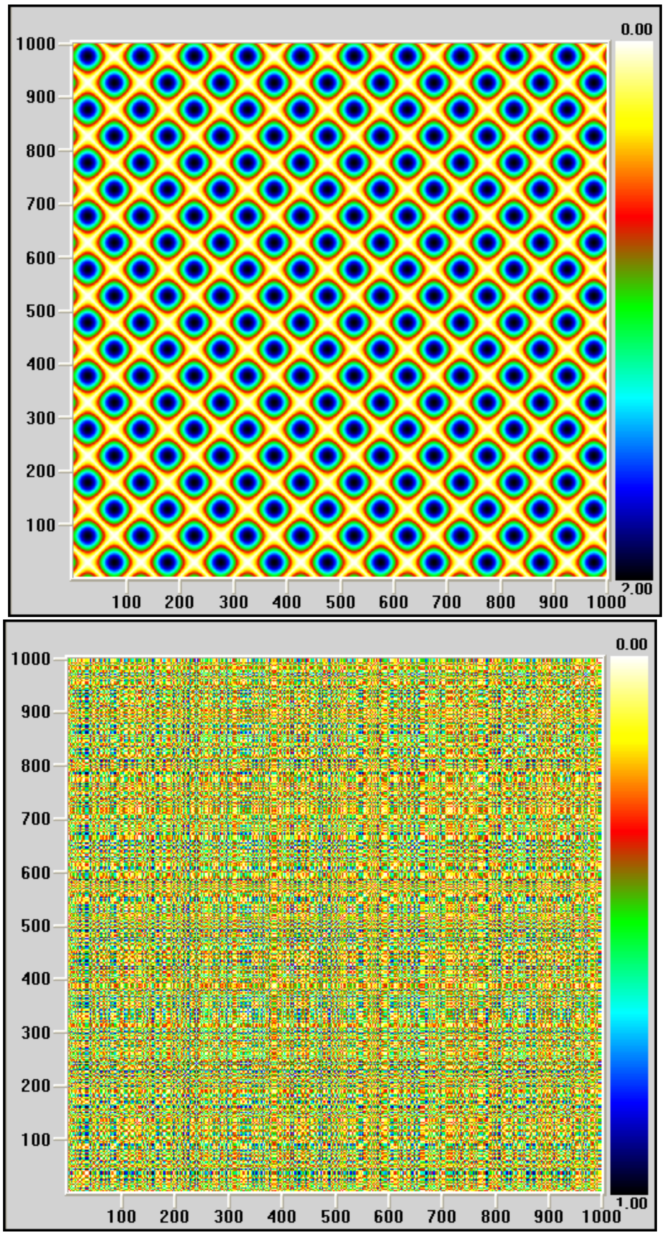

Figure 12. Recurrence plot using a data files included with VRA software. (top panel) In the RP organized patterns of color characteristics are shown for a periodic signal; sine wave with $STE = 0\%$. (bottom panel) In the RP an uniform distribution of color characteristics is shown for a random signal, white noise with $STE = 80\%$.

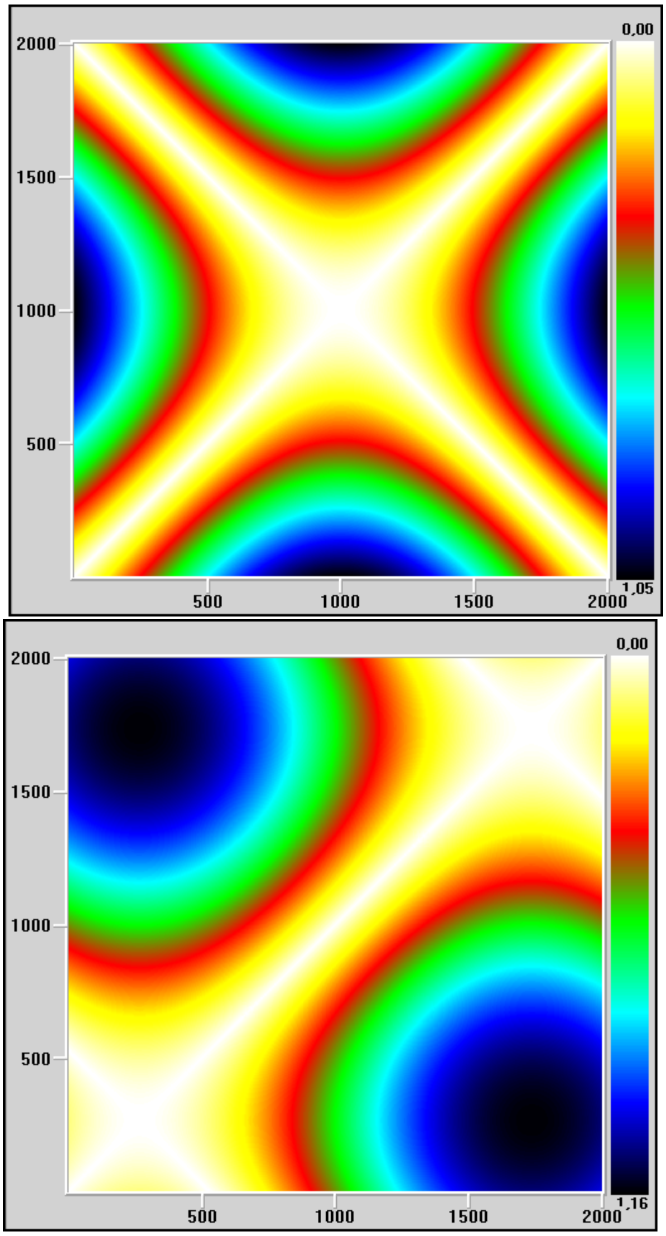

Figure 13. RPs of the solution for a cylindrically symmetric force-free field with constant alpha are shown. (top panel) Axial component : $B_A = B_0 J_0(\alpha R)$, $STE = 27\%$. (bottom panel) Tangential component : $B_T = B_0 H J_1(\alpha R)$, $STE = 0\%$.